ARP-T1 is a ciliary protein associated with a novel ciliopathy in inherited basal cell cancer, Bazex-Dupré-Christol Syndrome

Hyun-Sook Park[1], Christine Pich[1], Elena Chiticariu[1], Daniel Bachmann[1], Eirini Papanastasi[1], Gabriela Blanchard[1], Markus Plomann[2], Fanny Morice-Picard[3], Pierre Vabres[4], Asma Smahi[5,6], Marcel Huber[1] and Daniel Hohl[1,7]

[1]Department of Dermatology, CHUV-FBM UNIL, Hôpital de Beaumont, Lausanne, Switzerland
[2]Center for Biochemistry, University of Cologne, D-50931, Cologne, Germany
[3]Department of Dermatology, CHU, Hôpital Pellegrin, Bordeaux, France
[4]Department of Dermatology, CHU, Hôpital du Bocage, Dijon, France
[5]Paris Descartes University, Sorbonne Paris Cité, Paris, France
[6]IMAGINE Institute INSERM UMR 1163, Paris, France
[7]Lead Contact: daniel.hohl@chuv.ch

ABSTRACT

Actin-Related Protein-Testis1 (ARP-T1)/ *ACTRT1* gene mutations cause the Bazex-Dupré-Christol Syndrome (BDCS) characterized by follicular atrophoderma, hypotrichosis and basal cell cancer. Here, we report an ARP-T1 interactome involved in ciliogenesis, endosomal recycling and septin ring formation (PXD016557). Consequently, ARP-T1 localizes to the midbody during cytokinesis and the basal body of primary cilia in G_0. Tissue samples from BDCS patients show reduced ciliary length with significant correlations of ARP-T1 expression levels, confirmed by *ACTRT1* knock down. We report that BDCS is a novel ciliopathy and the first case of a skin cancer ciliopathy, where ARP-T1 plays a critical role to prevent pathogenesis.

INTRODUCTION

Basal cell cancer (BCC) of the skin is the most frequent human cancer. Bazex-Dupré-Christol Syndrome (BDCS) is an X-linked dominantly inherited syndrome form of BCC, without male-to-male transmission, affecting primarily the hair follicle (HF), and results in the triad of hypotrichosis, follicular atrophoderma and BCC [1-3]. Hypotrichosis and follicular atrophoderma develop around birth and BCC early in adulthood. BDCS less frequently presents with milia, hypohidrosis, facial pigmentation and trichoepithelioma, and thus combines developmental cutaneous anomalies with tumor predisposition, i.e. an ectodermal dysplasia with a hereditary tumor syndrome [4,5]. Unlike most cases of BCC, BDCS is an inherited syndromic form of BCC. The insertion mutation ARP-T1 547_548InsA creating a shift of the reading frame resulting in a truncated protein of 198 amino acids segregates with the disease, and germline mutations of non-coding sequences surrounding *ACTRT1* were identified and postulated to belong to enhancers transcribed as non-coding RNAs (eRNAs). ARP-T1 plays a role as a tumor suppressor in BDCS [6]. ARP-T1 was first isolated as a major acidic component of the cytoskeletal calix from the head of bull spermatozoa. ARP-T1 is expressed specifically late in spermatid differentiation in testis, where it locates to the postacrosomal region and the centriole [7], establishing a link to the primary cilium (PC) of epidermal cells implicated in the BCC development.

Cilia are microtubule-based organelles that are either motile as in sperm propel or nonmotile (primary) acting as sensory antenna, receiving signals from other cells nearby. The sensory capacity of PC is founded on the spatio-temporal localization of diverse receptor complexes such as PTCH, RTKs, TGFβR, NOTCH receptors, GPCRs including SMO, ion channels and extracellular matrix receptors along the cilium [8]. Ciliary communication is often compromised in cancer [9], and faulty Hedgehog signaling implicated in many cancers, prototypically in medulloblastoma and BCC. Indeed, BCC cells are frequently ciliated, and activated SHH signaling within primary cilia is a key driver in BCC pathogenesis [10]. BCCs generally show abnormal activation of the SHH signaling pathway, ascribing its constitutive activation as a prerequisite for the development of a BCC [11]. SHH signaling in its “off” state is characterized by PTCH1, repressing SMO activity. However, primary cilia have a dual role and are required for or may repress tumor formation [12,13] depending on the level of the molecular interaction [9].

PC assembly is a complex process emanating from the mother centriole with its appendages and differentiating upon cell cycle exit into the basal body, which nucleates the PC with apical CEP164 [14], a component of distal appendages, EHD1/EHD3 and SNAP29 [15] to initiate primary vesicle formation and ciliogenesis. Assembly of the primary cilium includes recruitment of periciliary membranes, transition zone components and a machinery of intraflagellar transport proteins to form the ciliary vesicle and to set the base for formation of the microtubular ciliary axoneme [15,16]. The PC is separated from the cytosol by the basal body and anchored by transition fibers/distal appendages in the ciliary pocket or periciliary plasma membrane (PM) [17]. Transition fibers and transition zone with its Y-shaped linkers serve as a ciliary gate for the cilio-cytoplasmic transport sharing some functional similarities with the nuclear pore complex [17,18]. Polarized membrane trafficking to the cilium and the vesicular transport machinery, which targets Golgi derived vesicles and apical recycling endosomes containing essential cargo, such as G protein-coupled receptors, to the periciliary PM or the ciliary pocket depends on small GTPases, notably RAB8 and RAB11, Rabin8 and the BBSome, a stable complex of seven proteins implicated in the ciliopathy of Bardet-Biedl Syndrome (BBS) [8].

Here, we demonstrate that ARP-T1 is a ciliary protein and involved in ciliogenesis by directly interacting with the ciliary machinery. Mutation in ARP-T1 as found in the tissues of BDCS patients and knock down of ARP-T1 gives rise to the abnormally shortened cilia caused by a disordered

actin cytoskeleton network. Ciliopathies encompass most human organ systems in eyes, nose, ears, organ placement, energy homeostasis, infertility, skeleton, reproductive system, brain, hydrocephalus, heart, chronic respiratory problems, kidney and liver [19]. We report that BDCS is the first ciliopathy of epidermal development and cancer.

RESULTS

ARP-T1 is expressed in differentiated human keratinocytes and human epithelial cells.

We examined the expression of ARP-T1 in normal human epidermal keratinocytes (NHEK) (Fig. 1a,b) and human immortalized keratinocytes HaCaT (Fig. 1c,d) cultured under differentiating conditions with high calcium up to seven days. The expression of ARP-T1 increased in a terminal differentiation dependent manner as indicated by the expression of Keratin 10 (K10) in differentiating keratinocytes at both mRNA (Fig. 1a,c) and protein levels (Fig. 1b,d, quantified in Extended data Fig. 1a,b). To investigate whether ARP-T1 expression was only induced in keratinocytes or whether it was related to differentiation, we also analyzed its expression in two differentiating retinal-pigmented epithelial cells, ARPE-19 (Fig. 1e,f) and hTERT-RPE1 (Fig. 1g,h). These cells were differentiated under serum starvation for 35 days or 48h respectively, assessed by the expression of the differentiation and ciliary protein IFT88 (Fig. 1f,h). Similar to keratinocytes, differentiated retinal-pigmented epithelial cells exhibited an increased ARP-T1 expression after differentiation, at both mRNA (Fig. 1e,g) and protein levels (Fig. 1f,h).

ACTRT1 is regulated by non-canonical hedgehog pathway and protein kinase C.

We previously reported that *ACTRT1* inhibits *GLI1* expression and is involved in hedgehog (HH) signaling [6]. We treated the hedgehog responsive hTERT-RPE1 cells with Smoothened (SMO) agonist (SAG) which binds to SMO and activates HH pathway, and measured the expressions of *ACTRT1* and HH pathway target genes, *GLI1* and *PTCH1*. The expression of *ACTRT1* mRNA was increased by SAG treatment in proliferating (Fig. 2a) and differentiating (Fig. 2b) conditions. Comparing both conditions, *ACTRT1* mRNA was further induced by SAG after differentiation and serum-starvation. *GLI1* and *PTCH1* mRNA responded well upon SAG treatment and did not show different expression in serum-starved cells (Fig. 2a,b). We used additional SMO activator, purmorphamine to confirm the results with SAG treatment, under differentiating condition. In this case, we also used vismodegib (Smoothened inhibitor used for the treatment of BCC) and both purmorphamine and vismodegib, to understand better the role of *ACTRT1* in HH pathway (Fig. 2c). *GLI1* (Fig. 2d) and *PTCH1* (Fig. 2e) mRNA expressions were used as controls of HH pathway activation. *ACTRT1* mRNA is induced 2.5 fold, *GLI1* and *PTCH1* mRNA about 2 fold upon purmorphamine treatment similar as the treatment with SAG. *GLI1* and *PTCH1* expression decreased upon both purmorphamine and vismodegib treatment as expected, but not the expression of *ACTRT1* indicating that *ACTRT1* mRNA expression is regulated by a non-canonical HH pathway.

A cascade of phosphorylation is known to be involved in HH signaling pathways, e.g. PKC, GSK-3β, S6K, PKA, PI3K, aPKC-ı/λ. To investigate the HH pathway in which *ACTRT1* plays a role for basal cell cancer, differentiated NHEK where *ACTRT1* is highly expressed, were treated with different kinase inhibitors. The cells treated with GF109203X known as PKC and PKA inhibitor showed significantly decreased expression of *ACTRT1* while cells treated with rapamycin (mTOR/S6K inhibitor), LY294002 (phosphoinositide-3-kinase inhibitor) and AG1478 (epidermal growth factor tyrosine kinase inhibitor) showed increased expression of *ACTRT1* (Fig. 2f). We

further narrowed down to treat NHEK and HaCaT cells with Gö6976 (PKC α/β inhibitor), Rottlerin (PKC δ inhibitor) and ZIP 2549 (atypical PKC inhibitor, a kind gift from Dr. Anthony Oro). We found that Rottlerin inhibits the expression of *ACTRT1* in both NHEK and HaCaT cells, indicating that *ACTRT1* mRNA expression is regulated by PKC δ (Fig. 2g,h).

Two different programs (PhosphositePlus and Swiss Institute of Bioinformatics) predicted several putative phosphorylation sites in ARP-T1 and ARP-T1 547_548insA (Fig. 2i). One of the predicted phosphorylation sites in C-terminus at S352 position showed similar consensus phosphorylation site specificity with PKC (www.kinexus.ca). We transduced ARP-T1 (W), ARP-T1 547_548insA (M) and vector control (V) tagged with DDK (same sequence as FLAG) into differentiated NHEK and immunoprecipitated using Anti-FLAG M2 affinity gel. We used Phospho-(Ser) PKC substrate antisera, which recognize proteins only when phosphorylated at serine residues surrounded by arginine or lysine at the -2 and +2 positions and a hydrophobic residue at the +1 position (ARP-T1 S352 : MSS*FKQ). This antisera recognized ARP-T1 but not ARP-T1 547_548insA suggesting that ARP-T1 is indeed phosphorylated by PKC and stable while ARP-T1 547_548insA is not phosphorylated by PKC, which lack the phosphorylation site, and therefore is prone to be degraded (Fig. 2j).

ARP-T1 interacts with proteins in ciliary machinery

To understand the molecular pathways exploited by ARP-T1, we performed co-immunoprecipitation followed by mass spectrometry analysis to identify proteins interacting with ARP-T1. We transduced ACTRT1 (W), ACTRT1 547_548insA (M) and vector control (V) tagged with DDK (same sequence as FLAG) into the cells and immunoprecipitated using anti-FLAG M2 beads. We found putative interacting proteins in HeLa cells (Fig. 3a), serum starved and differentiated hTERT-RPE1 cells (Fig. 3b), and NHEK (data not shown). ARP-T1 interacts in all cells with proteins involved in primary ciliary machinery. We confirmed these interactions by immunoblot analysis with acetylated Tubulin, TCP8 (one of 8 subunits of chaperonin-containing T-complex), Hsc70, BAG2, γ-Tubulin, EHD4, Septin2 and Septin9 antisera (Fig. 3a,b). While chaperones are often identified to some extent in MSA of precipitates with overexpressed proteins, the high number of spectral hits (Table 1) and the location of Septins and EHD4 at ciliary basal body lead us to observe the location of ARP-T1 in ciliated hTERT-RPE1 cells.

We analyzed ciliogenesis in ARPE-19 and hTERT-RPE1 cells, which was induced by serum starvation and differentiation. ARP-T1 localizes to the ciliary base forming a primary cilia structure when we co-stained ARP-T1 with acetylated Tubulin, which stains ciliary axoneme. ARP-T1 co-localized with Rootletin, a major basal body protein, in primary cilia (Fig. 3c and Extended data Fig. 1c in HaCaT cells). ARP-T1 interacts and forms a complex with γ-Tubulin, which localizes in the vicinity of the basal body (Fig. 3d and Extended data Fig. 1d in HaCaT cells). We also confirmed that ARP-T1 co-localizes with EHD4 and Septin2 (Fig. 3d). We used proximity ligation assays to further confirm these interactions (Extended data Fig. 1e and 1e). To reinforce these results, we choose to overexpress EHD4. We transfected hTERT-RPE1 cells with EHD4 (EHD4) and vector control (V) tagged with V5. After immunoprecipitation using anti-V5 beads and immunoblot, we detected ARP-T1 in the EHD4 samples but not in the vector control (Extended data Fig. 1g). In the same cells, we confirmed that ARP-T1 co-localizes with EHD4 (Extended data Fig. 1h).

ARP-T1 associates with a ciliopathy in BDCS

Based on the ciliary localization of ARP-T1 and the implication of Septin2 in ciliary length control [20], we analyzed the ciliary structures in the samples from BDCS patients (ACTRT1 547_548insA, Mutations B2, Mutation A3, Mutation CNE12 [6] comparing to the normal hair follicles and the samples from a sporadic BCC patient. First, we observed the ciliary structures by staining with Rootletin and acetylated Tubulin (Rootletin Ac-Tu DAPI in Fig. 4a, top) and confirmed co-localization of ARP-T1 and Rootletin (Rootletin ARP-T1 DAPI in Fig. 4a bottom, individual stainings with Rootletin, acetylated Tubulin or ARP-T1 are shown in Extended data Fig. 2 and 3). Strikingly, we observed a reduction of ciliary length (Fig. 4b) and fluorescence intensity of Rootletin and ARP-T1 (Fig. 4c,d) in the BDCS samples compared to the normal hair follicle and sporadic BCC. Ciliary length, Rootletin fluorescence and ARP-T1 fluorescence were particularly reduced in ACTRT1 547_548insA (insA in Fig. 4b-f) and B2 mutation while less prominently reduced in mutation A2 and CNE12. We also found significant correlations between ARP-T1 fluorescence and ciliary length (Fig. 4e) and between ARP-T1 fluorescence and Rootletin fluorescence (Fig. 4f). We concluded that BDCS, inherited BCC, unlike sporadic BCC, is a novel ciliopathy and the role of ARP-T1 as a part of cilia is to prevent the disease. To study the role of ARP-T1 in controlling ciliary length *in vitro*, we performed ARP-T1 knock down experiment in hTERT-RPE1 cells. We found that the lengths of cilia stained with acetylated Tubulin in *ACTRT1* knock down cells were reduced approximately 25% compared to control cells (Fig. 4g and shown by quantification in Fig. 4h) with 65% (KD1) and 50% (KD2) of knock down efficacy at *ACTRT1* mRNA (Fig. 4i) and ARP-T1 (Figure 4J) levels. These results were confirmed in HaCaT cells, in which cilia length was divided by two with 70% of ACTRT1 mRNA KD1 (Fig. 4k-n). Therefore, ARP-T1 is required for the maintaining of normal length of cilia *in vitro*. In sum, ARP-T1 is located in ciliary basal body and regulates ciliogenesis both *in vivo* and *in vitro.* Absence of ARP-T1 gives rise to an epidermal ciliopathy.

ARP-T1 is located in midbody in dividing cells.

It was reported that Septin 2 acts as a scaffold for myosin II and its kinases at the cleavage furrow [21] and that Septin 9 mediates midbody abscission during cytokinesis [22]. We, therefore, searched for the localization of ARP-T1 in dividing cells. ARP-T1 localized at the midbody in hTERT-RPE1 cells (Fig. 5a), HeLa cells (Fig. 5b) and HaCaT cells (Fig. 5c). Postmitotic midbody is directly implicated in primary ciliogenesis. After cytokinesis, the midbody remnant moves along the apical surface, proximal to the centrosome at the center of the apical surface where the primary cilium emerges. The midbody remnant carries Rab8, IFT20, IFT88 and exocyst subunits required for ciliogenesis. If the remnant is removed, primary ciliogenesis is greatly impaired [23]. Midbody remnant licenses primary cilia formation [24]. Both midbodies and primary cilia contain acetylated tubulin, many proteins in the midbody can also be found at the base of the cilium in the centrosome [25]. However, *ACTRT1* knock down has no obvious impact on cell division (data not shown).

DISCUSSION

Here, we report that ARP-T1 is a ciliary protein located at the basal body of primary cilia. BDCS tumors and ARP-T1 deficient RPE cells show shortened primary cilia. Thus, BDCS is a novel and first ciliopathy implicated in skin cancer caused by mutations of *ACTRT1*. ARP-T1 supports intact cilia and actin cytoskeleton network to control proper ciliogenesis. ARP-T1 is highly expressed during epidermal differentiation, is stabilized by protein kinase C and *ACTRT1* expression is regulated by protein kinase C δ and by a non-canonical Hedgehog pathway.

ACTRT1/ARP-T1 regulation has not been described yet. Here, we showed that HH and mTORC2/PKC delta pathways positively regulate *ACTRT1* at the mRNA level. HH signaling is activated upon cell differentiation, at the cilium, and is known to induce canonical and non-canonical pathways. As we previously reported that ARP-T1 activates the HH signaling [6], it was important to decipher a possible feedback loop with this pathway. We found that SMO activation favors *ACTRT1* mRNA expression. However a blockade with Vismodegib, drug used in the clinic to treat BCC patients, could not reverse Purmorphamine-induced *ACTRT1* mRNA. We concluded that *ACTRT1* is regulated by a non-canonical HH signaling. We next unraveled which phosphorylation pathway was implicated in this non-canonical HH signaling. MAP kinase inhibition with PD98059 had no effect on *ACTRT1* expression. By using PI3K/mTORC1/S6K and mTORC2/PKC delta inhibitors, we could demonstrate that the proliferating signaling PI3K/mTORC1/S6K limits *ACTRT1* expression while its differentiating counterpart mTORC2/PKC delta favors it. These findings highlight the role of HH and mTORC2/PKC delta pathways in *ACTRT1*/ARP-T1 regulation.

By MS analysis, we identified a machinery of molecular ARP-T1 interactors involved in PC formation (see Table 1): (1.) Chaperon containing TCP-1 (CCT/TRiC), consists of two identical stacked rings, each containing eight subunits (TCP1-8). The complex folds various proteins including actin and tubulin. It was shown that CCT/TRiC family chaperonin localizes to centrosomes and forms a complex with BBS proteins, BBS6, BBS10, and BBS12 and mediate the assembly of the BBSome, involved in ciliogenesis regulating transports of vesicles to the cilia [26]. This BBSome protein complex binds to Rabin8, the GTP/GDP exchange factor, for the small GTPase RAB8. RAB8 localizes to the cilium, is required for ciliogenesis, and mediates the docking and fusion of vesicles. It was proposed that the BBSome acts upstream of RAB8 in this vesicular transport to the cilium [27]. BBS causing IFT27 mutations point to a link of the BBSome with IFT where this small GTPase might be involved in delivering cargo from the BBSome to the IFT [28]; (2.) CCT and heat shock cognate 71 kDa protein (Hsc70) form a stable complex and this interaction was suggested to serve to deliver the unfolded substrate from Hsc70 to the substrate binding region of CCT [29]. Hsc 70 interacts with IFT88 [302]. Bcl2-associated athanogen (BAG2) protein forms a chaperone complex with Hsc70 and regulates their protein folding activity [31]; (3.) The Eps15 homology domain (EHD) family of proteins, composed of EHD1-4, is associated with Rab8 and Rab11 membranes and regulates endosomal membrane trafficking [32]. EHD4 locates to the transition zone of cilia and plays a role in protein transport to cilia and ciliogenesis. EHD4 deficient mice show a strong phenotype in skin, kidney and testis with small testis, reduced sperm motility, sperm number and germ cells, such that Ehd4-/- mice are subfertile. Approximately 50% of all EHD4-deficient mice suffer from reduced number of hairs (hypotrichosis) at the dorsal back and have a primary cilia phenotype (Dr. Markus Plomann, unpublished data); (4.) Septin2 localizes at the base of the axoneme. Cells completely depleted of Septin2 lack a cilium whereas cells partially depleted at the base of primary cilia have a significantly shorter cilium than control [20]. Septin2 interacts with Hsc70 [33]. Septin9 has been shown to interact with microtubules [34] and localizes to the ciliary pocket region [35]. Primary cilia in Septin9 depleted cells are shorter than that in control cells [36]. γ-Tubulin associates with centrosomes and localizes to the vicinity of basal body [37].

Overall, our MS results point to a function of ARP-T1 in the ciliary basal body at the crossroads of vesicle trafficking, protein folding and the cytoskeleton (Supplementary Table 1). The ciliary pocket or periciliary PM serves as an interface with the actin cytoskeleton, which is important for the movement of the basal body to the PM and for vesicular and endosomal trafficking [38 10 39,40]. We hypothesize that ARP-T1 is functional at this interface and may stabilize the cytoskeletal matrix.

Functional genomic screening showed that proteins involved in actin dynamics and endocytosis are important for ciliogenesis. Depletion of gelsolin family proteins (GSN and AVIL), which regulate cytoskeletal actin organization by severing actin filaments, reduced the number of ciliated cells and silencing of ACTR3 (ARP-3), a major constituent of the ARP2/3 complex involved in nucleating actin polymerization, increased cilium length [41]. On the other hand, it was reported that the actin cytoskeleton is disrupted in knockdown cell lines targeting ciliary proteins. For example, Ahi1, whose human ortholog is mutated in Joubert syndrome, knockdown cells showed disorganizing and decrease in actin filaments [42]. ARP-T1 has 49 % identity with β-actin and 40%, 37%, 29% identity with ARP-1, ARP-2, ARP-3, respectively. ARP-T1 as a ciliary protein is involved in a positive regulation of ciliogenesis. Similar case as ARP-T1, some cancer-associated mutations result in ciliary resorption. Von Hippel-Lindau (VHL) disease is characterized by the development of premalignant renal cysts, and arises because of functional inactivation of VHL tumor suppressor protein (pVHL). It maintains the structural integrity of the primary cilium for suppression of uncontrolled proliferation of kidney epithelial cells and cyst formation [43]. It was shown by electron microscopy that glioblastoma cells and tumors have immature primary cilia and basal body/centrioles [44] [45]. Mutations in Budding uninhibited by benzimidazole-related 1 (BUBR1), a molecule of spindle assembly checkpoint, cause premature chromatid separation (mosaic variegated aneuploidy), cancer disposition and impaired ciliogenesis [46].

With our results, we propose a model where ARP-T1 leads primary ciliogenesis via direct interaction with proteins in ciliary machinery. First, ARP-T1 presents in the mitotic spindle through the interaction with gamma Tubulin which presents in between the mother centriole and the daughter centriole (Fig. 5d). As the cytokinesis proceeds, the complex of ARP-T1 and two centriols moves to the central spindle where the midbody is formed by recruiting Septins (Fig. 5e). The midbody cleaves one side of intracellular bridge and remains tethered to one of the daughter cells. The complex of ARP-T1, two centriols and midbody move towards the apical surface of daughter cells where primary cilia will be formed (Fig. 5f,g).

Dynamic Hh signaling has been identified in mammalian post-natal testis, and SHH pathway components PTCH1, SUFU and GLI-1 were identified in spermatogonia, spermatocytes and spermatids [47], where spermatids express high levels of SUFU to repress SHH activity [48]. Interestingly, ARP-T1 locates to the centrosome in early stages of mouse testis differentiation and relocates to cytoplasm and cell membrane at later stages. We previously reported that ARP-T1 binds to the *GLI1* promoter and inhibits GLI1 mRNA expression signaling [6]. In this study, we showed that the elevated level of ARP-T1 with purmorphamine were not decreased by the treatment with purmorphamine and vismodegib (Fig. 2c-e). Thus, *ACTRT1* functions in a SMO independent HH pathway. The activation of a non-canonical HH pathway may explain the apparent paradox that we observed shortened primary cilia both in BCC from BCDS and in *ACTRT1* knocked down RPE cells. While loss of primary cilia is observed in diverse cancer where it correlates with worse prognosis, their retention is paramount for medulloblastoma and BCC development [9]. Nevertheless, SMO-independent operation occurs both in medulloblastoma [12] and BCC mouse models [13], and was recently linked to development of resistance to SMO-inhibition [49]. This suggest BDCS is a model for studying vismodegib resistance in BCC and medulloblastoma. We did not study the role of Ras/RhoA pathway, a second non-canonical HH signaling in ARP-T1 expression. Yet, it would an interesting target as it regulates the actin and cortactin cytoskeleton dynamics.

Our results show that ARP-T1 acts as a direct or indirect actor in a non-canonical HH pathway and bridges between actin cytoskeleton organization involved in vesicle transport at the

centrosome, the centrioles and the basal body, and the formation of primary cilia to prevent the pathogenesis of BDCS. Above all, our studies shed light on how ciliogenesis is controlled in carcinogenesis by ARP-T1. ARP-T1 could be a new target and novel therapeutic approaches in BDCS and BCC, the most frequent human cancer. This appears particularly important since loss of primary cilia as reported here in BDCS is a recognized mechanism of resistance to SMO inhibitors in medulloblastoma and BCC [49].

Online METHODS

Cell Culture and samples

Human neonatal foreskin keratinocytes (NHEK, established in our laboratory) and HaCaT cells (Invitrogen, Basel, Switzerland) were grown in EpiLife medium (Gibco, Invitrogen, Basel, Switzerland) with Human Keratinocyte Growth Supplement (Gibco, Invitrogen, Basel, Switzerland), 10 µg/ml gentamicin and 0.25 µg/ml amphotericin B (Gentamicin / Amphotericin B solution, Gibco, Invitrogen, Basel, Switzerland). ARPE-19 and hTERT-RPE1 (ATCC, Manassas, VA) cells were cultured in Dulbecco's Modified Eagle's Medium (DMEM) High Glucose, GlutaMAX™, Pyruvate (Gibco, Invitrogen, Basel, Switzerland) or DMEM/F12 (ATCC) with 0.01 mg/ml hygromycin B (Sigma-Aldrich, St Louis, MO), both media supplemented with 10% fetal bovine serum (FBS), 100 U/ml penicillin and 100 µg/ml streptomycin (BioConcept AG, Allschwil, Switzerland). HeLa and HEK293T (Invitrogen) were cultured in DMEM supplemented with 10% FBS, 100 U/ml penicillin and 100 µg/ml streptomycin. The cells were incubated at 37°C in a 5% CO2 atmosphere.

To induce cilia formation, NHEK and HaCaT were cultured up to 7 days in EpiLife media supplemented with 2 mM CaCl2. hTERT-RPE1 and ARPE-19 cells were cultured 48h or 35 days respectively in media containing 0.2% FBS.

Bazex-Dupré-Christol syndrome samples were collected and prepared as previously described in [6].

Lentivirus

Lentivirus particles for *ACTRT1* overexpression were produced with Calcium phosphate transfection method: *ACTRT1* wild-type (*WT*) and mutant containing the c.547-548InsA mutation constructs were produced as previously described in [6]. HEK293T cells were transiently co-transfected with psPAX2 (Addgene, Cambridge, MA) and pMD2.G (Addgene, Cambridge, MA) and empty vector or *ACTRT1* WT or mutant to produce lentiviral particles (*LVs*). LVs were harvested 48 hours later and the titer was determined in HeLa cells [50].

Lentiviral particles for *ACTRT1* shRNA were produced by Sigma-Aldrich, in pLKO backbone vector. ShRNA sequences are for ACTRT1 KD1: 5' CCG GGC CTG GTT TCT ACC TGT CTA ACT CGA GTT AGA CAG GTA GAA ACC AGG CTT TTT G 3', and ACTRT1 KD2: 5' CCG GGT GCC TTT AGC AAG ACT TAA TCT CGA GAT TAA GTC TTG CTA AAG GCA CTT TTT TG 3'. Control is an empty vector with same selection.

Viral transduction

HeLa, hTERT-RPE1 and HaCaT cells were transduced using polybrene (8 ug/mL, TR1003, Millipore), with lentivirus O/N at 37°C. The next day, lentivirus was removed and cells grew in their medium. Selection with puromycin (2.5 ug/mL, 540411, Calbiochem) or blasticidin (7.5 ug/mL, 15205, Sigma-Aldrich) started 24h later.

Drug Treatments

Cells were treated 24h with Smoothened agonists SAG (566660, Calbiochem) 200 and 400 nM and Purmorphamine (4551, Tocris bioscience) 3 uM, or antagonist Vismodegib (S1082, Selleckchem) 5 uM, or kinase inhibitors: GF109203X (ALX-270-049, Enzo Life Sciences) 10µM, SB431542 (1614, Tocris bioscience) 10µM, PD98059 (9900, Cell Signaling Technologies) 20µM, SP600125 (270-339-M005, Alexis Biochemicals) 5µM, SB216763 (1616, Tocris bioscience) 10µM, Rapamycin (R0161, LKT Laboratories) 200nM, LY294002 (70920, Cayman Chemical) 50µM, AG1478 (270-036-M001, Alexis Biochemicals) 5µM, Gö6976 (12060S, Cell Signaling Technologies) 3µM, Rottlerin (1610, Tocris bioscience) 10µM, ZIP (2549, Tocris bioscience, kind gift from Prof. Anthony Oro, Stanford University School of Medicine) 20µM.

Western blot

NHEK, HaCaT, ARPE-19, and hTERT-RPE1 cells were harvested in ice-cold FLAG (50 mM Tris/Cl pH 7.5, 150 mM NaCl, 1 mM EDTA, 1% Triton X-100, and protease inhibitor cocktail [Complete MiniTM tablette, Roche Diagnostics]) or RIPA (50 mM Tris/HCl pH 7.4, 150 mM NaCl, 12 mM Na deoxycholate, 1% NP-40, 0.1% SDS, protease inhibitor cocktail,and phosphatase inhibitor cocktail [PhosSTOP, PHOSS-RO, Roche]) lysis buffer for 30 min on ice with extensively pipetting every 10 min, then spun for 10 to 20 min at 12,000 x *g* at 4°C. Supernatants were collected, heated for 5 min at 85°C and centrifuged. Total protein concentration was determined by BCA assay (PierceTM BCA Protein Assay Kit; Thermo Scientific, Waltham, MA, USA). Fifteen ug of proteins were loaded onto a 10% SDS-PAGE gel and electroblotted onto a nitrocelulose or PVDF membrane membrane (Hybond ECL; Amersham, UK). Membranes were incubated with the following antibodies: anti-ARP-T1 (1:1000, SAB1408334, Sigma-Aldrich / 1:2000, GP-SH6, Progen), anti-Keratin 10 (1:200, MS-611-P0, Thermo Scientific), anti-βActin (loading control, 1:2000, A2066, Sigma-Aldrich) and anti-αTubulin (1:5000, T9026, Sigma-Aldrich). After washes in TBT-T, incubation with HRP-secondary antibodies (anti-mouse (1:5000, NA931V, GE Healthcare UK Limited), anti-rabbit (1:5000, NA934V, GE), anti-guinea pig (1:5000, ab97155, Abcam), and revelation with chemiluminescence, images were acquired using the Luminescent Image Analyzer LAS-4000 mini (Fujifilm, Tokyo, Japan). Band intensity was analyzed with Image J software (National Institutes for Health, USA).

Co-immunoprecipitation

Transduced HeLa, NHEK, and serum-starved hTERT-RPE1 cells were washed with PBS and harvested in the FLAG lysis buffer. Supernatants were incubated with 30 µl anti FLAG-beads (ANTI-FLAG™ M2 Affinity Gel) overnight at 4°C and 1h at room temperature (*RT*) on a rotator to pool-down ARP-T1-FLAG protein. Beads were separated by centrifugation for 3 min at 5000 x *g*, washed five times with TBS, and eluted in 23 µl TBS and 7 µl 5x SDS-sample buffer at 85°C for 5 min. ARP-T1 precipitation was confirmed using ARP-T1 antiserum (1:2000, Progen GP-SH6), and

co-precipitated protein were analyzed using anti-Acetylated-Tubulin (1:1000, T6793, Sigma-Aldrich), anti-TCP8 / TCP1 theta (1:500, PA5-30403, Thermo Scientific), anti-Hsc70 (1:200, PA5-27337, Thermo Scientific),anti-BAG2 (1:100, PA5-30922, Thermo Scientific), anti-gamma-tubulin (1:500, #ab11316, Abcam), anti-EDH4 (1:1000 kindly given by Prof. Plomann), anti-Septin2 (1:2000, HPA018481, Sigma-Aldrich), anti-Septin9 (1:2000, HPA042564, Sigma-Aldrich).

Proteomic analysis/ Mass Spectrometry

Transduced HeLa, NHEK, and serum--starved hTERT-RPE1 cells were washed with PBS and harvested in FLAG lysis buffer, and analyzed by the Proteomic Analysis Facility of University of Lausanne with the following protocol.

Gel separation and protein digestion

Protein samples were loaded on a 12 % mini polyacrylamide gel and migrated about 2.5 cm in non-reducing conditions. After Coomassie staining, gel lanes between 15-300 kDa were excised into 5-6 pieces, and digested with sequencing-grade trypsin (Promega) as described by Shevchenko and colleagues [51]. Extracted tryptic peptides were dried and resuspended in 0.05% trifluoroacetic acid, 2% (v/v) acetonitrile for mass spectrometry analyses.

Mass spectrometry analyses

Tryptic peptide mixtures were injected on a Dionex RSLC 3000 nanoHPLC system (Dionex, Sunnyvale, CA, USA) interfaced via a nanospray source to a high resolution mass spectrometer based on Orbitrap technology: Orbitrap Fusion Tribrid or QExactive Plus instrument (Thermo Fisher, Bremen, Germany), depending on the experiments considered. Peptides were loaded onto a trapping microcolumn Acclaim PepMap100 C18 (20 mm x 100 µm ID, 5 µm, Dionex) before separation on a C18 reversed-phase analytical nanocolumn, using a gradient from 4 to 76 % acetonitrile in 0.1 % formic acid for peptide separation (total time: 65min).

Q-Exactive Plus instrument was interfaced with an Easy Spray C18 PepMap column (25 cm x 75µm ID, 2µm, 100Å, Dionex). Full MS survey scans were performed at 70,000 resolution. In data-dependent acquisition controlled by Xcalibur software (Thermo Fisher), the 10 most intense multiply charged precursor ions detected in the full MS survey scan were selected for higher energy collision-induced dissociation (HCD, normalized collision energy NCE=27 %) and analysis in the orbitrap at 17’500 resolution. The window for precursor isolation was of 1.5 m/z units around the precursor and selected fragments were excluded for 60s from further analysis.

Orbitrap Fusion Tribrid instrument was interfaced with a reversed-phase C18 Nikkyo column (75 µm ID x 15 cm, 3.0 µm, 120Å, Nikkyo Technos, Tokyo, Japan) or a custom packed column (75 µm ID × 40 cm, 1.8 µm particles, Reprosil Pur, Dr. Maisch). Full survey scans were performed at a 120’000 resolution, and a top speed precursor selection strategy was applied to maximize acquisition of peptide tandem MS spectra with a maximum cycle time of 3s. HCD fragmentation mode was used at a normalized collision energy of 32%, with a precursor isolation window of 1.6 m/z, and MS/MS spectra were acquired in the ion trap. Peptides selected for MS/MS were excluded from further fragmentation during 60s.

Data analysis

MS data were analyzed using Mascot 2.5 (Matrix Science, London, UK) set up to search the Swiss-Prot (www.uniprot.org) database restricted to Homo sapiens taxonomy (UniProt, December 2015 version: 20'194 sequences). Trypsin (cleavage at K,R) was used as the enzyme definition, allowing 2 missed cleavages. Mascot was searched with a parent ion tolerance of 10 ppm and a fragment ion mass tolerance of 0.50 Da (Orbitrap Fusion) or 0.02 Da (QExactive Plus). Carbamidomethylation of cysteine was specified in Mascot as a fixed modification. N-terminal acetylation of protein and oxidation of methionine were specified as variable modifications.

Scaffold software (version 4.4, Proteome Software Inc., Portland, OR) was used to validate MS/MS based peptide and protein identifications, and to perform dataset alignment. Peptide identifications established at lower than 90.0% probability by the Scaffold Local FDR algorithm were filtered out. Protein identifications were accepted if they could be established at greater than 95.0% probability and contained at least 2 identified peptides. Protein probabilities were assigned by the Protein Prophet algorithm[52]. Proteins that contained similar peptides and could not be differentiated based on MS/MS analysis alone were grouped to satisfy the principles of parsimony. Proteins sharing significant peptide evidence were grouped into clusters.

The mass spectrometry proteomics data have been deposited to the ProteomeXchange Consortium [53] via the PRIDE [54] partner repository with the dataset identifier PXD016557 and 10.6019/PXD016557.

Immunofluorescence

Cells grown on coverslips were fixed in 4% formaldehyde/PBS for 20 min at RT, then permeabilized in 0.02% Triton-X/PBS for 10 min. Coverslips were incubated with blocking buffer containing 1% FBS and 2% bovine serum albumin (*BSA*) for 1h. Primary antibodies (anti-ARP-T1 (1:100, #SAB2103464; 1:200, Progen GP-SH6), anti-Acetylated-Tubulin (1:1000, T6793), anti-Rootletin (1:50, sc-67824, Santa-Cruz; 1:200, NBP1-80820, Novus), anti-gamma-tubulin (1:500, ab11316, Abcam), anti-EDH4 (1:200, kind gift by Prof. Plomann), anti-Septin2 (1:100, HPA018481, Sigma-Aldrich) were diluted in blocking buffer and applied on the cells for 2h at RT or overnight at 4°C. Coverslips were next incubated with secondary antibodies (1:500, A11008, A11001, A21467, A11035, A11003, A11060, Invitrogen; 1:100, BA-9500, Vector Laboratories; 1:200, RPN1233V, GE) for 1h at RT. Nucleus was stained with DAPI or Hoechst for 5 min at RT. Finally, coverslips were mounted onto slides with Dako mounting medium (Dako Schweitz AG, Baar, Switzerland) and examined with an inverted Zeiss LSM 700 laser scanning confocal microscope equipped with laser diode 405/488/555, SP490/SP555/LP560 emission filters, 2 PMT detectors and Zen2010 software (Zeiss, Feldbach, Switzerland).

Three-dimensional (3D) imaging technique was used to study ciliary imaging. Confocal images were captured at ~0.33-1 µm interval using 63 x/1.40 oil objectives. Using Image J software, the 3D structure was deconvoluded from the Z-stack, and the length, intensity and prevalence of cilia were manually traced and measured. Both cell number and proportion of cells exhibiting primary cilia were determined in approximately five representative fields (100 to 200 μm^2) for each experimental condition. The mean cilia prevalence was expressed as the percentage of ciliated cells. The average cilia length was expressed in µm. The ciliary rootlet was selected using the freehand tool and the average area was expressed in μm^2. The average pixel fluorescence intensity of proteins was quantified using the freehand tool to select the area of interest. Twenty to 50 cilia were measured for each experimental condition.

RNA extraction and Real time quantitative PCR.

Total RNA were harvested using the Qiagen RNeasy Mini Kit (Qiagen, Hombrechtikon, Switzerland) according to the manufacturer's instructions. RNA quantity and quality were assessed using the NanoDrop ND-1000 Spectophotometer (Wilmington, USA). RNA were reverse-transcribed using the Primescript RT reagent kit (TakaRa, Saint-Germain-en-Laye, France) in 10 µl reaction on a T-Gradient Thermocycler (Biometra, Biolabo, Châtel-St-Denis, Switzerland). Quantitative PCR (*qPCR*) was performed on cDNA with Power SYBRGreen PCR Mastermix (Applied Biosystems, CA, USA) on an Applied Biosystems StepOne thermal cycler (Applied Biosystems, Life Technologies, CA, USA). Gene expression was assessed by using *ACTRT1* (QT00215642, Qiagen), *GLI1* (Fw 5' AGA GGG TGC CAT GAA GCC AC 3', Rev 5' AAG GTC CCT CGT CCA AGC TG 3', Microsynth), *PTCH1* (Fw 5' GCT ACT TAC TCA TGC TCG CC 3', Rev 5' TCC GAT CAA TGA GCA CAG GC 3', Microsynth) primers. *RPL13A* (Fw 5'GCA TCC CAC CGC CCT ACG AC 3', Rev 5' CTC TTT CCT CTT CTC CTC CA 3', Microsynth) was used as endogenous control. Relative gene expression is normalized to the control and reported with a log2 scale.

Statistics/Data analysis

We used the one-way ANOVA or the Kruskal-Wallis test, depending on homogeneity of variances, to compare one independent variable in more than two groups. Linear regression was used to compare the correlation between two parameters.

To compare gene expression quantified by RT-qPCR, for each gene, all samples were normalized to the control, and log-2 transformed fold changes comparison to 0 were performed with a one-sample t test. To compare protein expression, all samples were normalized to the control, and fold changes comparison to 1 were performed with a one-sample t test.

All statistical analyses were performed using Prism GraphPad (v8, La Jolla, CA, USA).

ACKNOWLEDGEMENTS

We are thankful to Professor Rune Toftgard and to Professor Anthony Oro for their kind advice. We also acknowledge the Protein Analysis Facility of the University of Lausanne for the mass spectrometry assay. This study was funded by Swiss National Science Foundation (grant 310030-173102), "Fondation Professeur Placide Nicod" and "Fondation Dind Cottier pour la recherche sur la peau".

REFERENCES

1. Bazex, A., Dupre, A. & Christol, B. [Follicular atrophoderma, baso-cellular proliferations and hypotrichosis]. *Ann Dermatol Syphiligr (Paris)* **93**, 241-254 (1966).

2. Parren, L.J. & Frank, J. Hereditary tumour syndromes featuring basal cell carcinomas. *Br J Dermatol* **165**, 30-34 (2011).

3. Vabres, P.*, et al.* The gene for Bazex-Dupre-Christol syndrome maps to chromosome Xq. *J Invest Dermatol* **105**, 87-91 (1995).

4. Abuzahra, F., Parren, L.J. & Frank, J. Multiple familial and pigmented basal cell carcinomas in early childhood - Bazex-Dupre-Christol syndrome. *J Eur Acad Dermatol Venereol* **26**, 117-121 (2012).

5. Castori, M., Castiglia, D., Passarelli, F. & Paradisi, M. Bazex-Dupre-Christol syndrome: an ectodermal dysplasia with skin appendage neoplasms. *Eur J Med Genet* **52**, 250-255 (2009).

6. Bal, E.*, et al.* Mutations in ACTRT1 and its enhancer RNA elements lead to aberrant activation of Hedgehog signaling in inherited and sporadic basal cell carcinomas. *Nat Med* **23**, 1226-1233 (2017).

7. Heid, H.*, et al.* Novel actin-related proteins Arp-T1 and Arp-T2 as components of the cytoskeletal calyx of the mammalian sperm head. *Exp Cell Res* **279**, 177-187 (2002).

8. Schou, K.B., Pedersen, L.B. & Christensen, S.T. Ins and outs of GPCR signaling in primary cilia. *EMBO Rep* **16**, 1099-1113 (2015).

9. Liu, H., Kiseleva, A.A. & Golemis, E.A. Ciliary signalling in cancer. *Nat Rev Cancer* **18**, 511-524 (2018).

10. Briscoe, J. & Therond, P.P. The mechanisms of Hedgehog signalling and its roles in development and disease. *Nat Rev Mol Cell Biol* **14**, 416-429 (2013).

11. Kasper, M., Jaks, V., Hohl, D. & Toftgard, R. Basal cell carcinoma - molecular biology and potential new therapies. *J Clin Invest* **122**, 455-463 (2012).

12. Han, Y.G.*, et al.* Dual and opposing roles of primary cilia in medulloblastoma development. *Nat Med* **15**, 1062-1065 (2009).

13. Wong, S.Y.*, et al.* Primary cilia can both mediate and suppress Hedgehog pathway-dependent tumorigenesis. *Nat Med* **15**, 1055-1061 (2009).

14. Schmidt, K.N.*, et al.* Cep164 mediates vesicular docking to the mother centriole during early steps of ciliogenesis. *J Cell Biol* **199**, 1083-1101 (2012).

15. Lu, Q.*, et al.* Early steps in primary cilium assembly require EHD1/EHD3-dependent ciliary vesicle formation. *Nat Cell Biol* **17**, 531 (2015).

16. Kim, J.*, et al.* Actin remodelling factors control ciliogenesis by regulating YAP/TAZ activity and vesicle trafficking. *Nat Commun* **6**, 6781 (2015).

17. Reiter, J.F., Blacque, O.E. & Leroux, M.R. The base of the cilium: roles for transition fibres and the transition zone in ciliary formation, maintenance and compartmentalization. *EMBO Rep* **13**, 608-618 (2012).

18. Roberson, E.C.*, et al.* TMEM231, mutated in orofaciodigital and Meckel syndromes, organizes the ciliary transition zone. *J Cell Biol* **209**, 129-142 (2015).

19. Reiter, J.F. & Leroux, M.R. Genes and molecular pathways underpinning ciliopathies. *Nat Rev Mol Cell Biol* **18**, 533-547 (2017).

20. Hu, Q.*, et al.* A septin diffusion barrier at the base of the primary cilium maintains ciliary membrane protein distribution. *Science* **329**, 436-439 (2010).

21. Joo, E., Surka, M.C. & Trimble, W.S. Mammalian SEPT2 is required for scaffolding nonmuscle myosin II and its kinases. *Dev Cell* **13**, 677-690 (2007).

22. Estey, M.P., Di Ciano-Oliveira, C., Froese, C.D., Bejide, M.T. & Trimble, W.S. Distinct roles of septins in cytokinesis: SEPT9 mediates midbody abscission. *J Cell Biol* **191**, 741-749 (2010).

23. Bernabe-Rubio, M.*, et al.* Novel role for the midbody in primary ciliogenesis by polarized epithelial cells. *J Cell Biol* **214**, 259-273 (2016).

24. Ott, C.M. Midbody remnant licenses primary cilia formation in epithelial cells. *J Cell Biol* **214**, 237-239 (2016).

25. Smith, K.R.*, et al.* A role for central spindle proteins in cilia structure and function. *Cytoskeleton (Hoboken)* **68**, 112-124 (2011).

26. Seo, S.*, et al.* Controlling superconductivity by tunable quantum critical points. *Nat Commun* **6**, 6433 (2015).

27. Nachury, M.V.*, et al.* A core complex of BBS proteins cooperates with the GTPase Rab8 to promote ciliary membrane biogenesis. *Cell* **129**, 1201-1213 (2007).

28. Aldahmesh, M.A.*, et al.* IFT27, encoding a small GTPase component of IFT particles, is mutated in a consanguineous family with Bardet-Biedl syndrome. *Hum Mol Genet* **23**, 3307-3315 (2014).

29. Cuellar, J.*, et al.* The structure of CCT-Hsc70 NBD suggests a mechanism for Hsp70 delivery of substrates to the chaperonin. *Nat Struct Mol Biol* **15**, 858-864 (2008).

30. Bhowmick, R.*, et al.* Photoreceptor IFT complexes containing chaperones, guanylyl cyclase 1 and rhodopsin. *Traffic* **10**, 648-663 (2009).

31. Takayama, S., Xie, Z. & Reed, J.C. An evolutionarily conserved family of Hsp70/Hsc70 molecular chaperone regulators. *J Biol Chem* **274**, 781-786 (1999).

32. Zhang, J., Naslavsky, N. & Caplan, S. Rabs and EHDs: alternate modes for traffic control. *Biosci Rep* **32**, 17-23 (2012).

33. Tokhtaeva, E.*, et al.* Septin dynamics are essential for exocytosis. *J Biol Chem* **290**, 5280-5297 (2015).

34. Mostowy, S. & Cossart, P. Septins: the fourth component of the cytoskeleton. *Nat Rev Mol Cell Biol* **13**, 183-194 (2012).

35. Kukic, I., Rivera-Molina, F. & Toomre, D. The IN/OUT assay: a new tool to study ciliogenesis. *Cilia* **5**, 23 (2016).

36. Ghossoub, R.*, et al.* Septins 2, 7 and 9 and MAP4 colocalize along the axoneme in the primary cilium and control ciliary length. *J Cell Sci* **126**, 2583-2594 (2013).

37. Muresan, V., Joshi, H.C. & Besharse, J.C. Gamma-tubulin in differentiated cell types: localization in the vicinity of basal bodies in retinal photoreceptors and ciliated epithelia. *J Cell Sci* **104 (Pt 4)**, 1229-1237 (1993).

38. Benmerah, A. The ciliary pocket. *Curr Opin Cell Biol* **25**, 78-84 (2013).

39. Malicki, J.J. & Johnson, C.A. The Cilium: Cellular Antenna and Central Processing Unit. *Trends Cell Biol* **27**, 126-140 (2017).

40. Uddin, B., *et al.* The human phosphatase CDC14A modulates primary cilium length by regulating centrosomal actin nucleation. *EMBO Rep* **20**(2019).

41. Kim, J., *et al.* Functional genomic screen for modulators of ciliogenesis and cilium length. *Nature* **464**, 1048-1051 (2010).

42. Hsiao, Y.C., *et al.* Ahi1, whose human ortholog is mutated in Joubert syndrome, is required for Rab8a localization, ciliogenesis and vesicle trafficking. *Hum Mol Genet* **18**, 3926-3941 (2009).

43. Thoma, C.R., *et al.* pVHL and GSK3beta are components of a primary cilium-maintenance signalling network. *Nat Cell Biol* **9**, 588-595 (2007).

44. Moser, J.J., Fritzler, M.J. & Rattner, J.B. Primary ciliogenesis defects are associated with human astrocytoma/glioblastoma cells. *BMC Cancer* **9**, 448 (2009).

45. Moser, J.J., Fritzler, M.J. & Rattner, J.B. Ultrastructural characterization of primary cilia in pathologically characterized human glioblastoma multiforme (GBM) tumors. *BMC Clin Pathol* **14**, 40 (2014).

46. Miyamoto, T., *et al.* Insufficiency of BUBR1, a mitotic spindle checkpoint regulator, causes impaired ciliogenesis in vertebrates. *Hum Mol Genet* **20**, 2058-2070 (2011).

47. Sahin, Z., *et al.* Dynamic Hedgehog signalling pathway activity in germline stem cells. *Andrology* **2**, 267-274 (2014).

48. Makela, J.A., *et al.* Hedgehog signalling promotes germ cell survival in the rat testis. *Reproduction* **142**, 711-721 (2011).

49. Zhao, X., *et al.* A Transposon Screen Identifies Loss of Primary Cilia as a Mechanism of Resistance to SMO Inhibitors. *Cancer Discov* **7**, 1436-1449 (2017).

50. Almeida, S., Ryser, S., Obarzanek-Fojt, M., Hohl, D. & Huber, M. The TRAF-interacting protein (TRIP) is a regulator of keratinocyte proliferation. *J Invest Dermatol* **131**, 349-357 (2011).

51. Shevchenko, A., Tomas, H., Havlis, J., Olsen, J.V. & Mann, M. In-gel digestion for mass spectrometric characterization of proteins and proteomes. *Nat Protoc* **1**, 2856-2860 (2006).

52. Nesvizhskii, A.I., Keller, A., Kolker, E. & Aebersold, R. A statistical model for identifying proteins by tandem mass spectrometry. *Anal Chem* **75**, 4646-4658 (2003).

53. Deutsch, E.W., *et al.* The ProteomeXchange consortium in 2017: supporting the cultural change in proteomics public data deposition. *Nucleic Acids Res* **45**, D1100-D1106 (2017).

54. Perez-Riverol, Y., *et al.* The PRIDE database and related tools and resources in 2019: improving support for quantification data. *Nucleic Acids Res* **47**, D442-D450 (2019).

FIGURES:

Figure 1. ARP-T1 is expressed during epidermal and epithelial differentiation.
a,**c**,**e**,**g**, mRNA expression of ACTRT1 during the differentiation of keratinocytes, NHEK (**a**, N=5) and HaCaT (**c**, N=2), and epithelial cells, ARPE19 (**e**, N=3) and hTERT-RPE1 (**g**, N=5). Data are

presented as means ±S.D of the fold change compared to the value of undifferentiated samples. **b**,**d**,**f**,**h**, ARP-T1 expression during the differentiation of keratinocytes, NHEK (**b**) and HaCaT (**d**), and epithelial cells, ARPE19 (**f**) and hTERT-RPE1 (**h**). ARP-T1 was detected using guinea pig anti-ARP-T1 antisera (**b**) or rabbit antibody (**d**,**f**,**h**). * indicates polymers of ARP-T1 confirmed by mass spectrometry analysis. Keratin 10 and IFT88 were used as markers of cell differentiation in keratinocytes and epithelial cells respectively, actin and alpha-tubulin as loading controls.

Figure 2. *ACTRT1* is regulated by non-canonical Hedgehog signaling pathway and by Protein Kinase Cδ.
a,**b**, Relative *ACTRT1*, *GLI1* and *PTCH1* mRNA expression upon treatment with SAG in hTERT-RPE1 cells under proliferative (**a**) and differentiating (**b**) conditions (N=6). **c**-**e** Relative *ACTRT1* (**c**, N=7), *GLI1* (**d**, N=4), *PTCH1* (**e**, N=3) mRNA expression upon treatment with Purmorphamine and/or Vismodegib in differentiated hTERT-RPE1 cells. **f**,**g**, Relative *ACTRT1* mRNA expression upon treatment with different protein kinase inhibitors (**f**) or with PKC inhibitors (**g**) in differentiated NHEK (N=3). **h**, Relative *ACTRT1* mRNA expression upon treatment with PKC inhibitors in differentiated HaCaT cells (N=3). Data are presented as means ±S.D of the fold change compared to the value of DMSO treated samples.

Figure 3. ARP-T1 interacts with proteins involved in ciliary machinery
a,**b**, HeLa (**a**) and hTERT-RPE1 (**b**) cells were transduced with Lentiviral vectors V (pLCMV-Myc-DDK), M (pLCMV-547_548InsA-Myc.DDK) and WT (pLCMV-ACTRT1-Myc-DDK), and immunoprecipitated (IP) with anti-FLAG (DDK) monoclonal antibody M2-conjugated agarose, and analyzed by immuno blot (IB) with indicated antisera**. c**, Immunofluorescence stainings of ARP-T1, Acetylated tubulin and Rootletin in 35 days of serum-starved ARPE19 cells. Nuclei are stained with DAPI. Scale bar, 5 µm. Higher magnifications of the boxed area are shown on right three panels. Scale bar, 1 µm. **d**, Immunofluorescence staining of ARP-T1, γ-Tubulin, EHD4, and Septin 2 in 48 hours of serum-starved hTERT-RPE1 cells Nuclei are stained with DAPI. Scale bar, 5 µm. Higher magnifications of the boxed area are shown on right three panels. Scale bar, 1 µm.

Figure 4. The Bazex-Dupré-Christol syndrome is a ciliopathy caused by ARP-T1 and knock down of ACTRT1 in hTERT-RPE1 cells induces resorption of primary cilia.
a, Representative immunofluorescence images using Acetylated tubulin (green) and Rootletin (red) (left) and ARP-T1 (green) and Rootletin (red) (right) in hair follicle, sporadic BCC and 4 BDCS (ACTRT1 547_548insA, Mutation B2, Mutation A3, Mutation CNE described in [6]). Cell nuclei are stained with DAPI (blue). Scale bar, 5 µm. **b**, Quantification of the ciliary length (µm) from 3D confocal immunofluorescence microscopy images. **c**,**d**, Quantification of the relative fluorescence intensity of Rootletin (**c**, N=5) and ARP-T1 (**d**, N=10) on the ciliary rootlet. **b**-**d**, Results are represented as Tukey box-plot. Open circles represent outliers. **e**,**f**, Correlation between the ARP-T1 fluorescence and ciliary length (**e**), and between the ARP-T1 and Rootletin fluorescence (**f**). **g**, Immunofluorescence stainings of Acetylated tubulin (red) and Rootletin (green) in 48 hours of serum starved control and *ACTRT1* knock down hTERT-RPE1 cells. Cell nuclei are stained with DAPI (blue). **h**,**i**, Quantification of the ciliary length (**h**) and relative expression of *ACTRT1* mRNA (**I**, N=3) in control and *ACTRT1* knock down hTERT-RPE1 cells. **j**, Expression of ARP-T1 in control and *ACTRT1* knock down hTERT-RPE1 cells. **k**, Immunofluorescence stainings of Acetylated tubulin (green) and Rootletin (red) in 7 days differentiated control and *ACTRT1* knock down HaCaT cells. Cell nuclei are stained with Hoechst (blue). **l**,**m**, Quantification of the ciliary length (**l**) and relative expression of *ACTRT1* mRNA (**m**, N=3) in control and *ACTRT1* knock down HaCaT cells. **n**, Expression of ARP-T1 in control and *ACTRT1* knock down HaCaT cells. For cilia length, 20 to 50 cilia in two independent experiments in cells.

Figure 5. ARP-T1 localizes to midbody during cytokinesis
a, Immunofluorescence stainings of ARP-T1 (red) and Acetylated tubulin (green) in hTERT-RPE1 cells. Cell nuclei are stained with DAPI (blue). **b**, Immunofluorescence stainings of ARP-T1 (green)

and Acetylated tubulin (red) in HeLa cells. Cell nuclei are stained with DAPI (blue). **c**, Immunofluorescence stainings of ARP-T1 (red) and Acetylated tubulin (green) in HaCaT cells. Cell nuclei are stained with DAPI (blue). **d**-**g**, Model for ARP-T1 travelling from midbody to the primary cilium.

SUPPLEMENTARY METHODS

In situ proximity-mediated ligation assay (PLA)

hTERT-RPE1 cells were seeded on coverslips, fixed and permeabilized. Duolink in situ PLA kit with anti-rabbit PLUS probe and anti-mouse or anti-goat MINUS probe (Sigma-Aldrich, St Louis, MO, USA) was used according to manufacturer`s instructions: blocking for 30 min in a 37°C humidified chamber, incubation with primary antibodies (γ-tubulin (1:500, ab11316), ARP-T1 (1:100, SAB2103464), rootletin (1:50, sc-67824), EHD4 (1:200, ab83859, Abcam), septin-2 (1:100, HPA018481, Sigma-Aldrich), septin-9 (1:100, HPA042564, Sigma-Aldrich) for 2h at RT or overnight at 4°C, hybridization with PLA PLUS and MINUS probes (1:5 dilution) for 1h at 37°C, ligation, amplification and final washes. Nucleus was stained with DAPI for 2 min at RT. Coverslips were mounted onto slides and complex formation was examined with an inverted Zeiss LSM 700 microscope.

SUPPLEMENTARY LEGENDS

Extended data Fig.1. ARP-T1 localization in HaCaT cells and interactions in hTERT-RPE1 cells.
a,**b**, Quantification of ARP-T1 expression in ARPE19 (**a**) and hTERT-RPE1 (**b**) (N=3). **c**,**d**, Immunofluorescence stainings of ARP-T1 (red) and Acetylated tubulin (Ac-Tu, green) (**c**) and ARP-T1 (red) and γ-tubulin (Ga-Tu, green) (**d**) in 7 days differentiated HaCaT cells. Nuclei are stained with DAPI (blue). Higher magnifications of the boxed area are shown on right three panels. **e**, Proximity-mediated ligation assays using ARP-T1 and Rootletin, or γ-tubulin (Ga-Tu), or EHD4, or Septin 2 (SEPT2), or Septin 9 (SEPT9) antibodies, in 48h serum-starved hTERT-RPE1 cells. **f**, Proximity-mediated ligation assays using ARP-T1, Rootletin, γ-tubulin (Ga-Tu), EHD4, Septin 2 (SEPT2), or Septin 9 (SEPT9) antibody alone, in 48h serum-starved hTERT-RPE1 cells. **g**, hTERT-RPE1 cells were transfected with EHD4 (pcDNA6-V5-EHD4) and empty vectors (pcDNA6-V5), serum starved for 48 hours, and immunoprecipitated (IP) with anti-V5 antibody-conjugated agarose, and analyzed by immunoblot (IB) with indicated antibodies. **h**, Immunofluorescence stainings of ARP-T1 (red) and EHD4 (green). Nuclei are stained with Hoechst (blue).

Extended data Fig.2. Acetylated tubulin and Rootletin stainings in patient samples.
Representative immunofluorescence images using Acetylated tubulin (green) and Rootletin (red) in hair follicle, sporadic BCC and 4 BDCS (ACTRT1 547_548insA, Mutation B2, Mutation A3, Mutation CNE described in [6]). Cell nuclei are stained with DAPI (blue). Scale bar, 5 µm.

Extended data Fig.3. ARP-T1 and Rootletin stainings in patient samples.
Representative immunofluorescence images ARP-T1 (green) and Rootletin (red) (right) in hair follicle, sporadic BCC and 4 BDCS (ACTRT1 547_548insA, Mutation B2, Mutation A3, Mutation CNE described in [6]) using Acetylated tubulin (green) and Rootletin (red). Cell nuclei are stained with DAPI (blue). Scale bar, 5 µm.

AUTHOR CONTRIBUTIONS

Nature Medicine requires an Author Contribution statement as described in the Authorship section of our Editorial policies.

COMPETING INTERESTS

Submission of a signed Competing Interests Statement is required for all content of the journal. This statement will be published at the end of Letters, Articles, Reviews and Progress articles, whether or not a competing interest is reported. In the interests of transparency and to help readers form their own judgements of potential bias, Nature Research journals' require authors to declare any competing financial and/or non-financial interests in relation to the work described. The corresponding author is responsible for submitting a competing interests' statement on behalf of all authors of the paper.

Park_Fig. 1

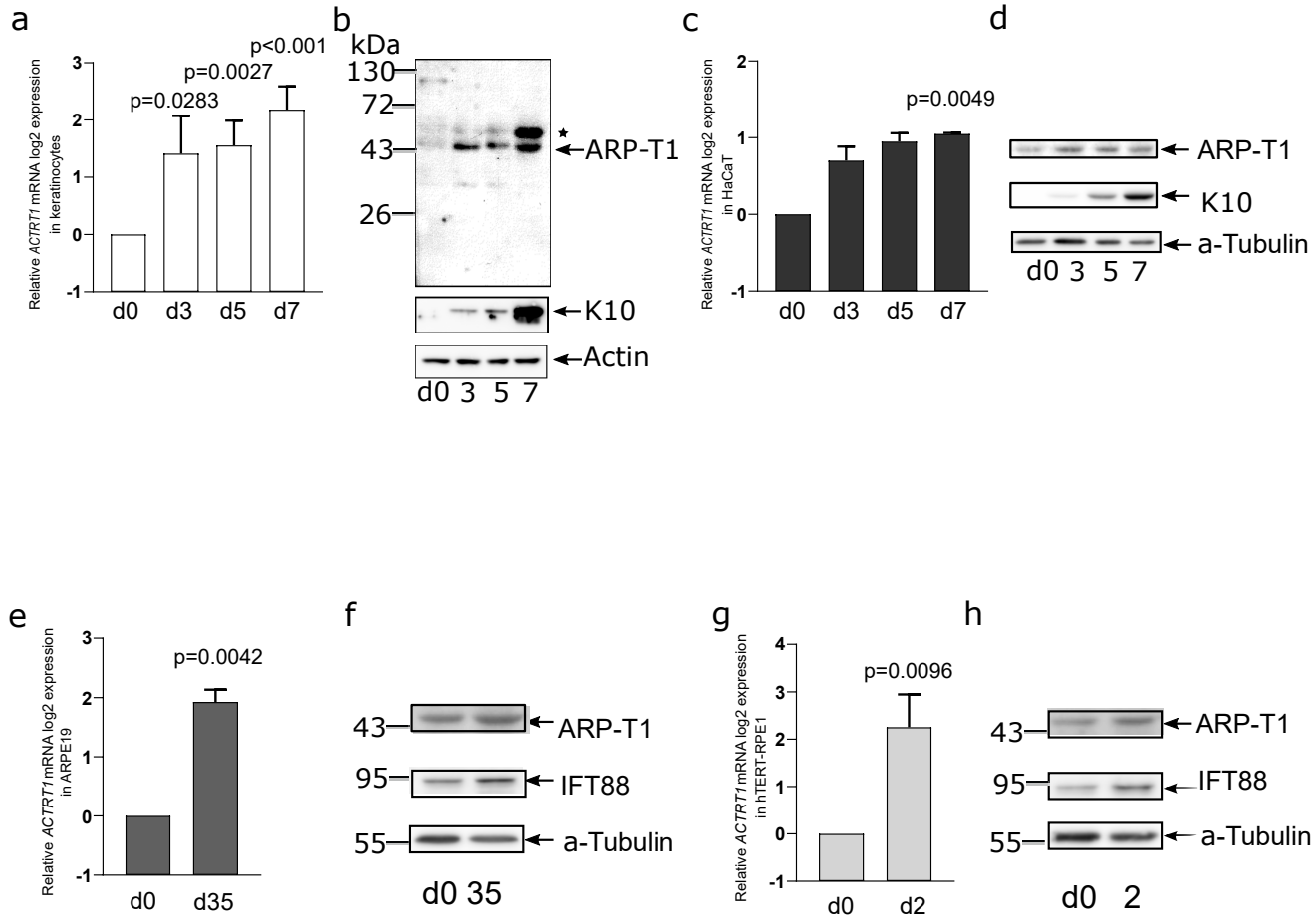
a
Relative ACTRT1 mRNA log2 expression in keratinocytes
p=0.0283
p=0.0027
p<0.001
d0
d3
d5
d7
b
kDa
130
72
43
26
ARP-T1
K10
Actin
d0 3 5 7
c
Relative ACTRT1 mRNA log2 expression in HaCaT
p=0.0049
d0
d3
d5
d7
d
ARP-T1
K10
a-Tubulin
d0 3 5 7
e
Relative ACTRT1 mRNA log2 expression in ARPE19
p=0.0042
d0
d35
f
43
95
55
ARP-T1
IFT88
a-Tubulin
d0 35
g
Relative ACTRT1 mRNA log2 expression in hTERT-RPE1
p=0.0096
d0
d2
h
43
95
55
ARP-T1
IFT88
a-Tubulin
d0 2

Park_Fig. 2

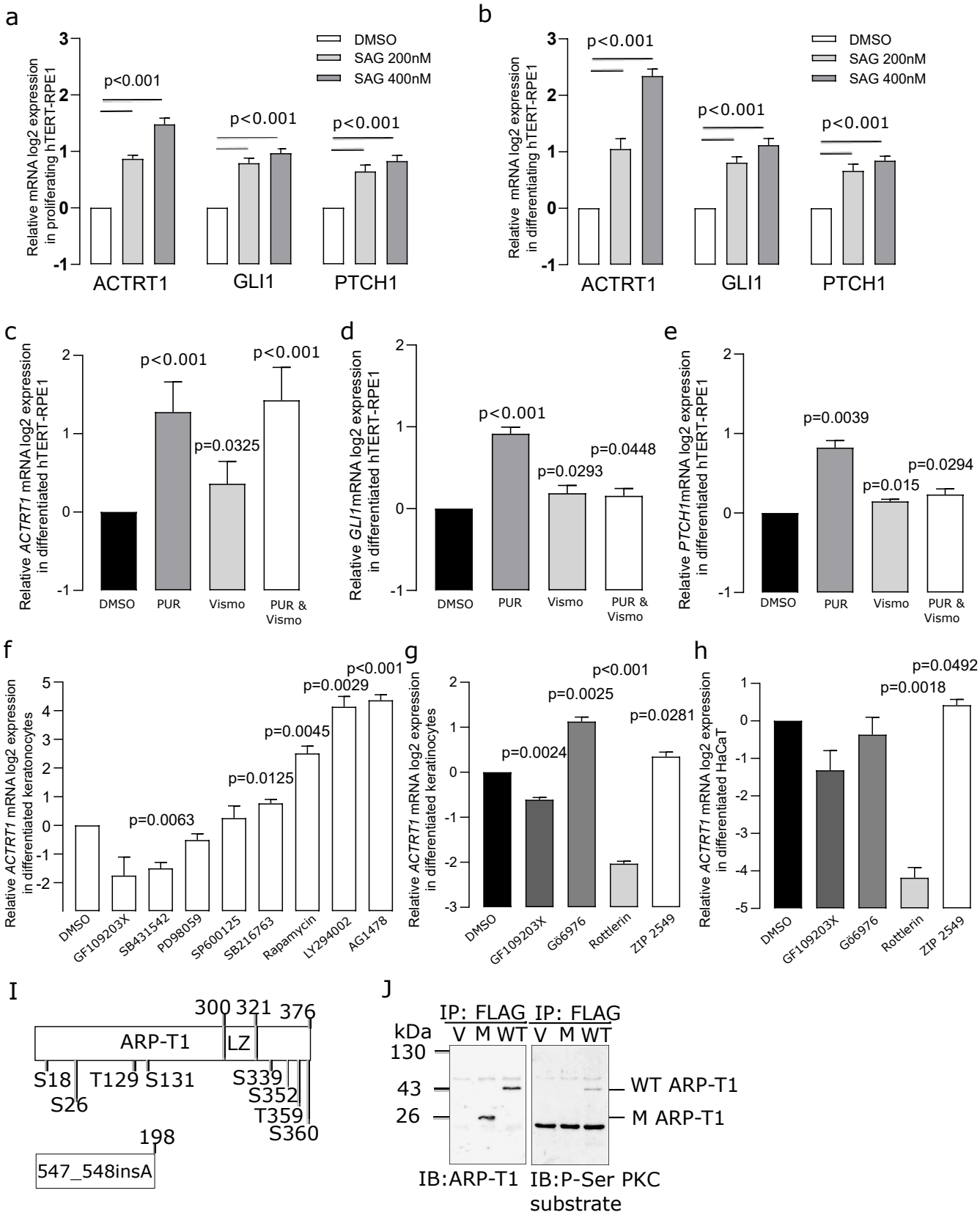
a
Relative mRNA log2 expression in proliferating hTERT-RPE1
DMSO
SAG 200nM
SAG 400nM
p<0.001
p<0.001
p<0.001
ACTRT1
GLI1
PTCH1
b
Relative mRNA log2 expression in differentiating hTERT-RPE1
p<0.001
p<0.001
p<0.001
c
Relative ACTRT1 mRNA log2 expression in differentiated hTERT-RPE1
p<0.001
p=0.0325
p<0.001
DMSO
PUR
Vismo
PUR & Vismo
d
Relative GLI1mRNA log2 expression in differentiated hTERT-RPE1
p<0.001
p=0.0293
p=0.0448
e
Relative PTCH1mRNA log2 expression in differentiated hTERT-RPE1
p=0.0039
p=0.015
p=0.0294
f
Relative ACTRT1 mRNA log2 expression in differentiated keratonocytes
p=0.0063
p=0.0125
p=0.0045
p=0.0029
p<0.001
DMSO
GF109203X
SB431542
PD98059
SP600125
SB216763
Rapamycin
LY294002
AG1478
g
Relative ACTRT1 mRNA log2 expression in differentiated keratinocytes
p=0.0024
p=0.0025
p<0.001
p=0.0281
DMSO
GF109203X
Gö6976
Rottlerin
ZIP 2549
h
Relative ACTRT1 mRNA log2 expression in differentiated HaCaT
p=0.0018
p=0.0492
DMSO
GF109203X
Gö6976
Rottlerin
ZIP 2549
I
300 321 376
ARP-T1
LZ
S18
S26
T129
S131
S339
S352
T359
S360
198
547_548insA
J
IP: FLAG
IP: FLAG
kDa
V M WT V M WT
130
43
26
WT ARP-T1
M ARP-T1
IB:ARP-T1
IB:P-Ser PKC substrate

Park_Fig 3

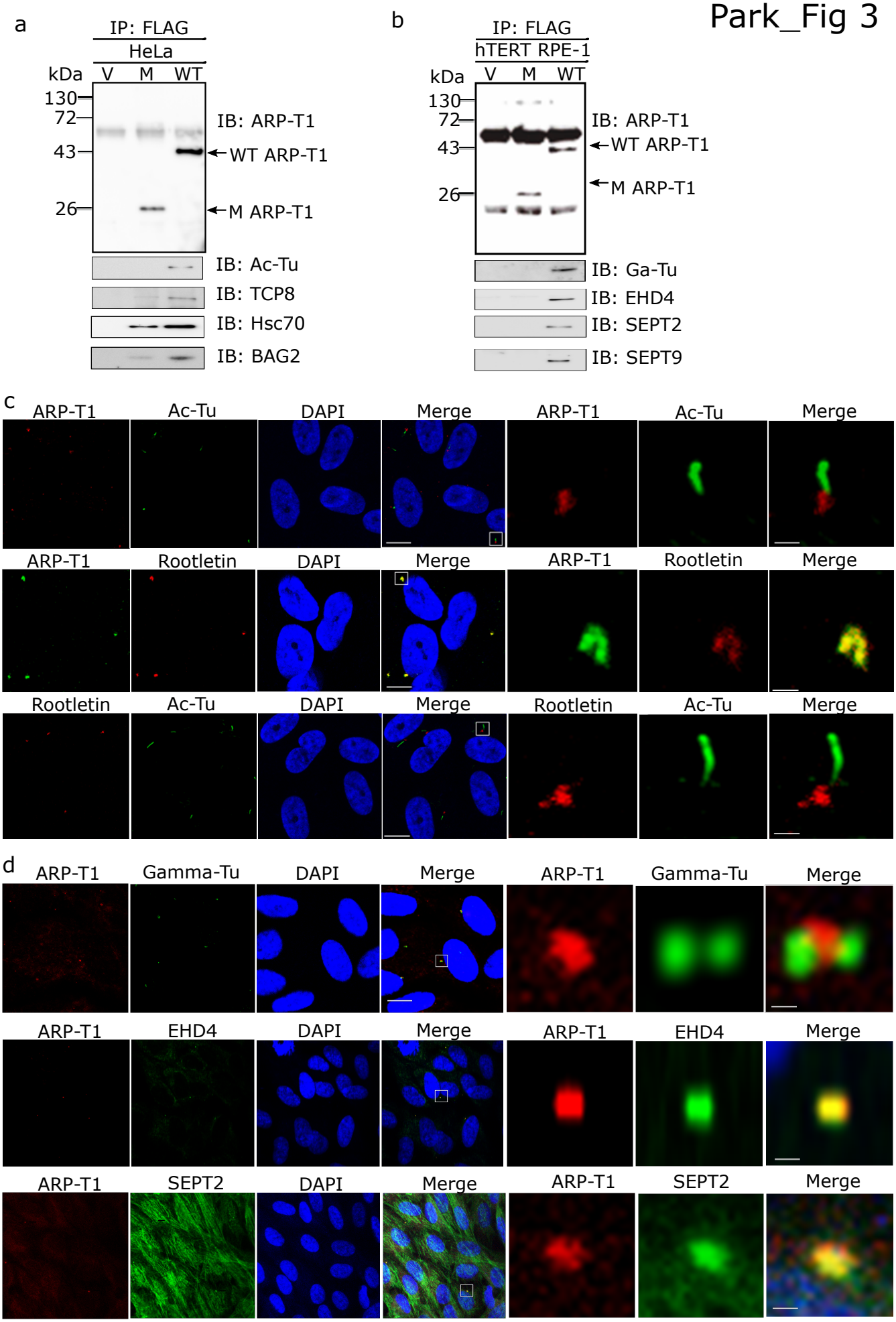
a
IP: FLAG
HeLa
kDa
V
M
WT
130
72
43
26
IB: ARP-T1
WT ARP-T1
M ARP-T1
IB: Ac-Tu
IB: TCP8
IB: Hsc70
IB: BAG2
b
IP: FLAG
hTERT RPE-1
kDa
V
M
WT
130
72
43
26
IB: ARP-T1
WT ARP-T1
M ARP-T1
IB: Ga-Tu
IB: EHD4
IB: SEPT2
IB: SEPT9
c
ARP-T1
Ac-Tu
DAPI
Merge
ARP-T1
Ac-Tu
Merge
ARP-T1
Rootletin
DAPI
Merge
ARP-T1
Rootletin
Merge
Rootletin
Ac-Tu
DAPI
Merge
Rootletin
Ac-Tu
Merge
d
ARP-T1
Gamma-Tu
DAPI
Merge
ARP-T1
Gamma-Tu
Merge
ARP-T1
EHD4
DAPI
Merge
ARP-T1
EHD4
Merge
ARP-T1
SEPT2
DAPI
Merge
ARP-T1
SEPT2
Merge

Park_Fig 4

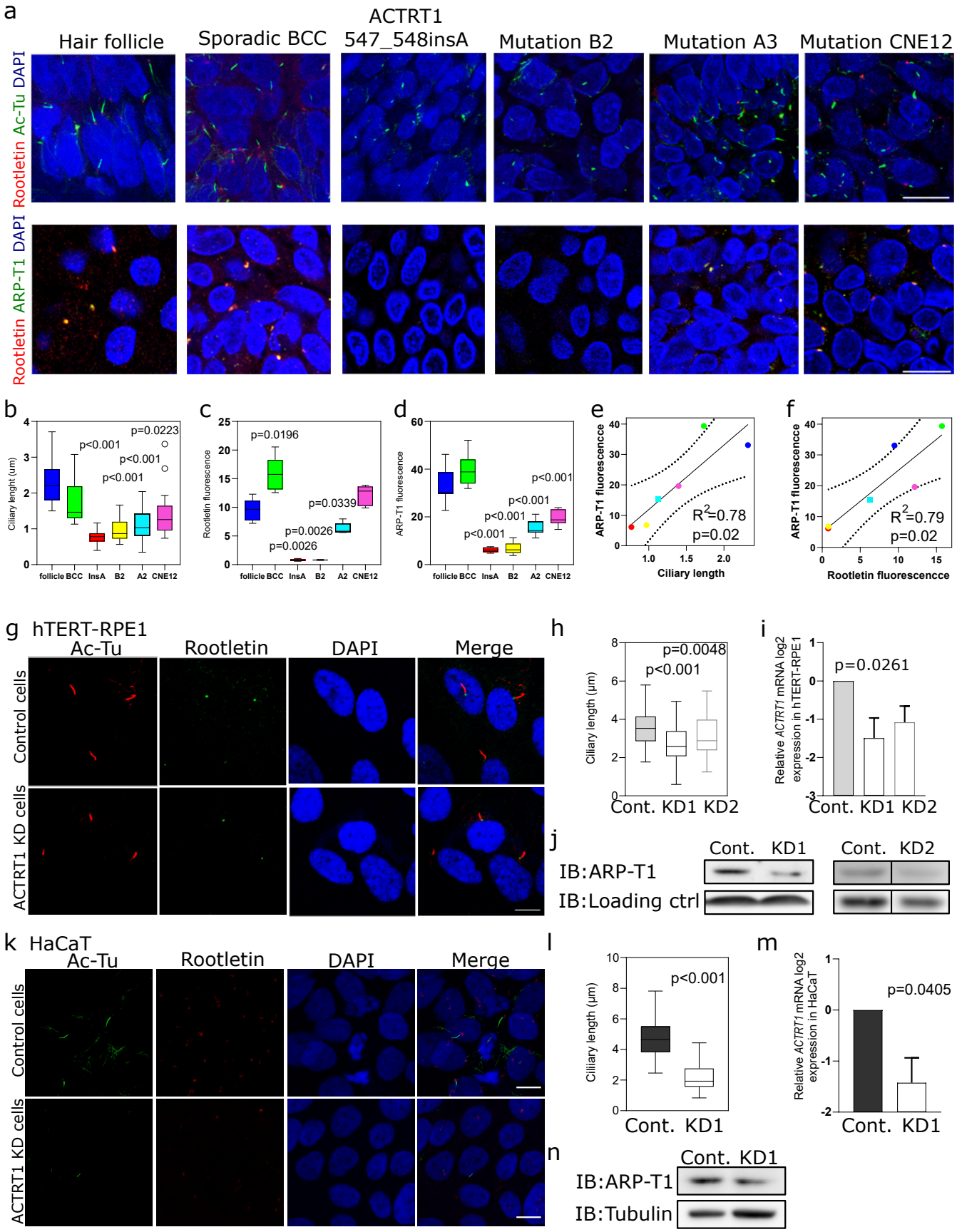
a
Hair follicle
Sporadic BCC
ACTRT1 547_548insA
Mutation B2
Mutation A3
Mutation CNE12
Rootletin Ac-Tu DAPI
Rootletin ARP-T1 DAPI
b
Ciliary lenght (um)
p=0.0223
p<0.001
p<0.001
p<0.001
follicle BCC InsA B2 A2 CNE12
c
Rootletin fluorescence
p=0.0196
p=0.0339
p=0.0026
p=0.0026
follicle BCC InsA B2 A2 CNE12
d
ARP-T1 fluorescence
p<0.001
p<0.001
p<0.001
p<0.001
follicle BCC InsA B2 A2 CNE12
e
ARP-T1 fluorescencce
Ciliary length
R2=0.78
p=0.02
f
ARP-T1 fluorescencce
Rootletin fluorescencce
R2=0.79
p=0.02
g hTERT-RPE1
Ac-Tu
Rootletin
DAPI
Merge
Control cells
ACTRT1 KD cells
h
Ciliary length (µm)
p=0.0048
p<0.001
Cont. KD1 KD2
i
Relative ACTRT1 mRNA log2 expression in hTERT-RPE1
p=0.0261
Cont. KD1 KD2
j
Cont. KD1
Cont. KD2
IB:ARP-T1
IB:Loading ctrl
k HaCaT
Ac-Tu
Rootletin
DAPI
Merge
Control cells
ACTRT1 KD cells
l
Ciliary length (µm)
p<0.001
Cont. KD1
m
Relative ACTRT1 mRNA log2 expression in HaCaT
p=0.0405
Cont. KD1
n
Cont. KD1
IB:ARP-T1
IB:Tubulin

Park_Fig 5

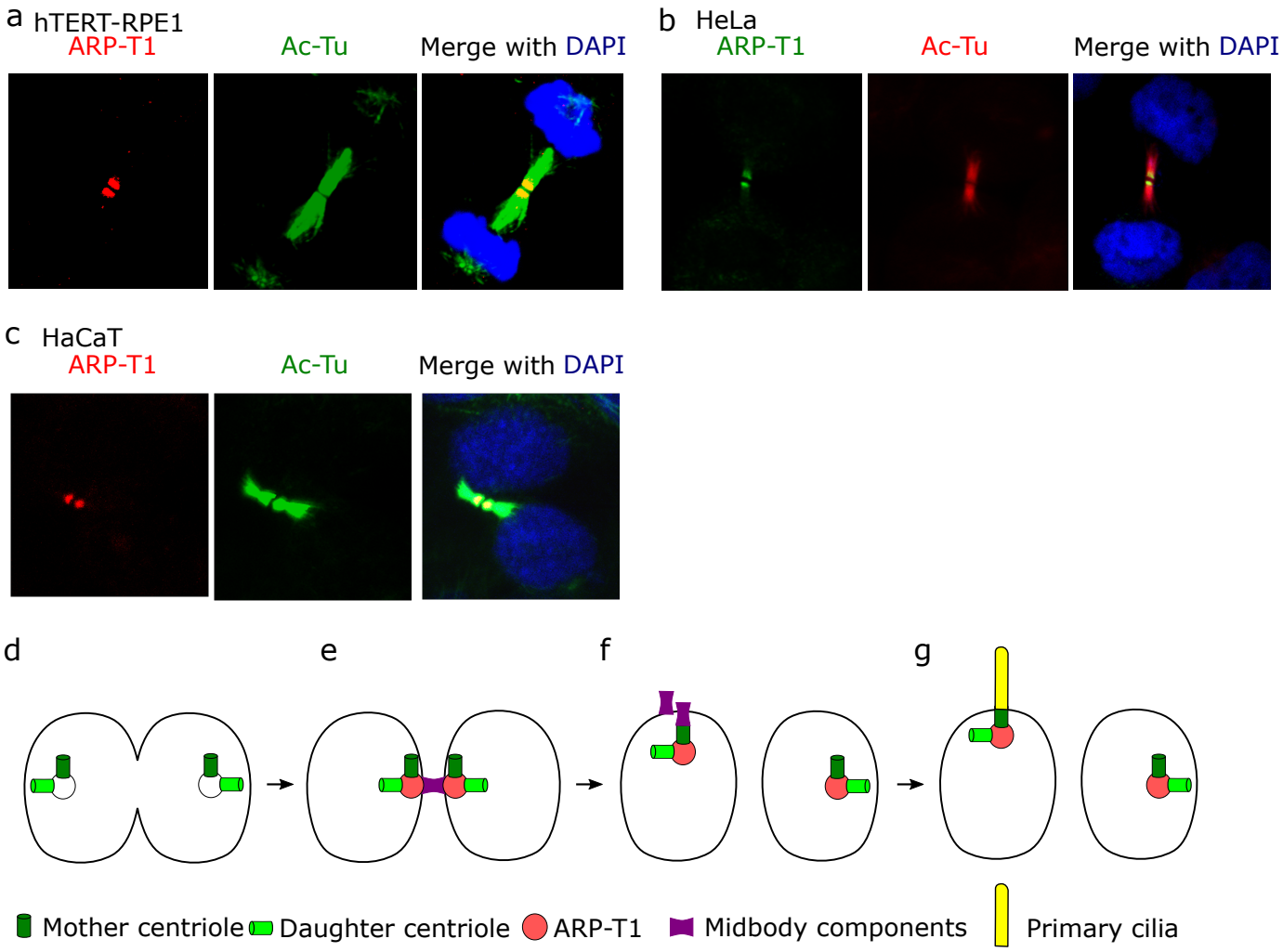
a hTERT-RPE1
ARP-T1
Ac-Tu
Merge with DAPI
b HeLa
ARP-T1
Ac-Tu
Merge with DAPI
c HaCaT
ARP-T1
Ac-Tu
Merge with DAPI
d
e
f
g
Mother centriole
Daughter centriole
ARP-T1
Midbody components
Primary cilia

HeLa cells	**ARP-T1**	**547_548 InsA**	**Vector**
ARP-T1	183	91	0
Heat shock cognate 71 kDa protein	121	68	9
T-complex protein 1 subunit theta (TCP1 theta)	66	20	0
RuvB-like 2	73	39	1
Erlin-2	28	16	0
BAG family molecular chaperone regulator 2 (BAG 2)	91	33	4
Ras-related protein Rab-8A	7	4	0
Dynactin	19	3	0
Importin subunit α-1	18	7	0
Exportin 1	19	2	0
Filamin-A	11	5	0
hTERT-RPE			
BAG2	45	14	1
TCP1 theta	19	0	0
RuvB-like 1	14	4	0
EH domain containing protein 4 (EHD4)	16	1	0
Septin-2	12	2	1
Septin-9	6	1	0
Rab10	10	3	1
PDZ and LIM domain protein 5 (PDLI5)	10	0	0
Rab6A	5	0	0
EH domain containing protein 1 (EHD1)	5	0	0
Actin related protein 2	4	1	0
Cortactin	11	9	4

Table 1